Local buckling resistance of Pultruded FRP columns: Theoretical predictions vs. Experimental study

Nguyen Tien Thuy

STASD Research Group, Ho Chi Minh City University of Transport
Email: thuy.nguyen@ut.edu.vn (Corresponding author)

Abstract:

Fiber-Reinforced Polymer (FRP) in the form of thin-walled plate structures are widely used in different engineering applications due to their outstanding features such as: high strength-to-weight ratio, excellent fatigue and corrosion resistance, etc. Due to the low stiffness, design of FRP material is usually governed by deformations or instabilities, rather than strengths. The development of a technical specification for design of FRP composite structures requires the understanding on buckling behaviour of FRP components. Local buckling of pultruded FRP column is a type of structural instabilities, occurs when the compressive stress reaches to the level that form waves in the flanges or web plates, causing the plastic deformation in the fiber which ultimately reduces its strength and stiffness. This study focuses on the local buckling resistance of pultruded FRP columns by experimental work. The test data were compared to current theoretical and numerical predictions. It is found that the difference of <15% between experiment and predictions can be acceptable. The author recommends that the Kollar's equations to be used when predicting local buckling of Pultruded FRP column of I or channel shapes.

Keywords: Local buckling; Abaqus; Experimental study; Theoretical predictions.

1. Introduction

Fibre-Reinforced Polymer (FRP) composites are widely used in various engineering applications across the world for the last couple of decades. Their exceptional features such as: High strength, low weight, high resistance to fatigue, corrosion, etc., have made them popular structural materials in the marine and aerospace industries. In addition, FRPs are the preferred structural material in civil engineering works due to desirable mechanical properties, allow for cost reduction, high durability and prefabricable. The transportation infrastructure sector, such as bridges, tunnel linings, underground culverts, and sheet piles, is among the application areas that have benefited from FRP composites as a viable construction material.

Local buckling is a type of structural instability occurs when either the plate of flanges or web buckled (depending on which critical local buckling stress reaches first), resulting in the formation of wave shapes as illustrated in Figure 1. Unlike global buckling, which results in the failure of column or beam immediately after buckling, local buckling allows for the column to withstand higher loads until ultimate failure. This type of instability typically occurs in stocky (short) beams or columns. In contrast, long and slender components are more prone to lateral-torsional buckling or Euler's buckling at a much lower load. Having the feature of high strength and low elastic moduli, the Pultruded FRP (PFRP) structures can be more sensitive to buckling failure compare to thin-walled structures made of steel. This behavior has been studied by several researchers, leading to the proposal of different closed-form equations for the prediction of flanges or web buckling.

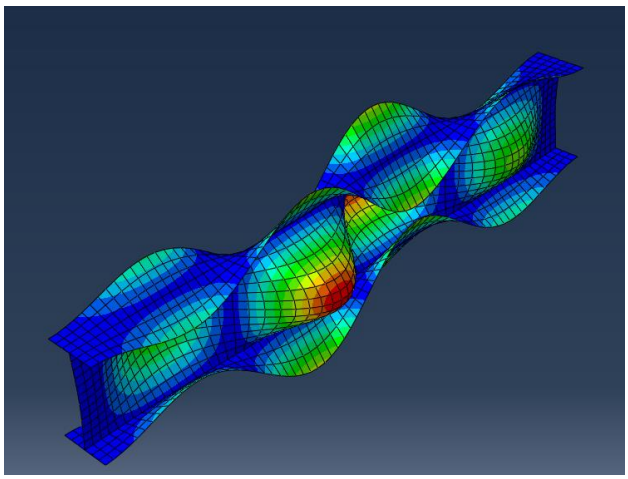

Figure 1. Photo of local buckling showing "wave" on flanges and web.

Mottram [1] evaluated nine available equations and recommended that the critical local buckling stress can be calculated as:

$$f_{cr} = G_{LT}\left(\frac{2t_f}{b}\right)^2 \quad (1)$$

Where the G_{LT} is the shear modulus; t_f is the flange thickness and b is the breadth of the section.

It can be seen that this equation is only suitable for section having long plate with large aspect ratios (length/width). Also, the stiffness between web and flange junction was not taken into account.

Kollar [2] proposed a set of closed-form equations in which the influence of web-flange junction stiffness has been considered. The equations require for the calculation of flanges and web independently in order to predict which plate to fail first, from which the local buckling stress of beam or column can be determined.

Cardoso et al. [3] develops equation for an infinitely long plate to accommodate the critical half-wave length to determine the local buckling stress of I-sections made of orthotropic material.

Ragheb [4] conducted a series of comprehensive parametric study, and the results were used in a regression analysis to develop closed-form equation for the predictions of local buckling resistance of several pultruded shapes. The proposed equation seems to be complicated and inconvenient in practice.

Recently, Liu et al. [5] adopted classic plate theory and the energy method to propose an explicit equation for local flange buckling. A modified buckling factor is proposed.

In practice, the author finds that the closed-form equation proposed by Kollar [2] to be most convenient.

In this paper, the author concentrates on investigating the local buckling resistance of pultruded FRP column by experimental work and compare the test results with the prediction formula by Kollar [2]. The finding of this research would be useful for researchers or code writers when looking for suitable ways to approximate the local buckling resistance of beam or column, using in the definition of non-dimensional slenderness λ_{LT} for design purpose. This research would also provide more test data that could then can be used to calibrate the design factor in a design code for FRP composite structures.

2. Theoretical predictions

The elastic critical buckling stress that causes a panel in a section to become unstable depends on the displacement boundary conditions along the longitudinal edges and the load arrangement on the transverse edges as shown in Figure 2.

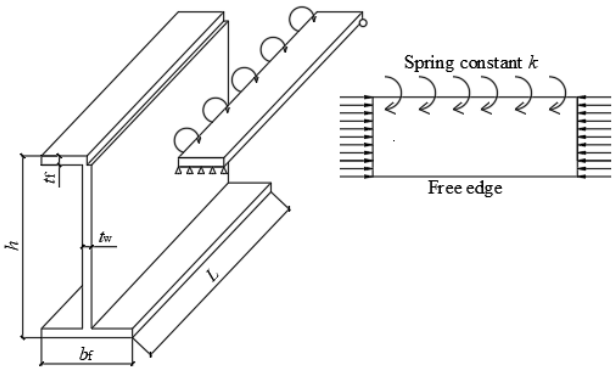

Figure 2. Boundary and load condition for flange outstand plate.

For I and channel sections, the flange outstands have one free edge while the other is restrained at the web-flange junction (Figure 2), while the web in these shapes is restrained along both sides. In wide-flange I and channel shapes where $h = b_f$ (see Figure 3) local flange buckling normally occurs prior to web buckling [6]. This might not be the case if the section is of the narrow-flange type (h≥ $2b_f$).

A closed-form equation for the approximation of the local flange stress for I section can be given as [2], [6]:

$$\sigma_{\text{Loc,flange}} = \frac{\pi^2}{t_f \left(b_f / 2\right)^2}\left[D_L \left(\frac{b_f / 2}{a}\right)^2 + \frac{12}{\pi^2} D_s \right] \quad (2)$$

By replacing $b_f/2$ in eq. (2) with b_f, the local flange stress for the channel shape is obtained. In eq. (2) b_f is the breadth of the section and a is the buckling half-wave length.

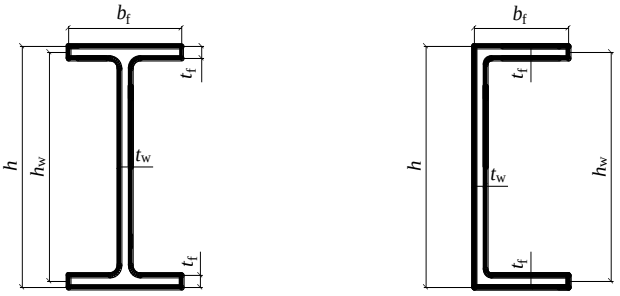

(a) I-section (b) Channel section

Figure 3. Illustration for I and Channel sections.

For the web, the local buckling stress can be expressed by:

$$\sigma_{\text{Loc,web}} = \frac{2\pi^2}{t_w {b_w}^2}\left(\sqrt{D_L D_T} + D_{LT} + 2D_s\right) \quad (3)$$

Where D_L, D_T, D_{LT} and D_s are the flexural rigidities of the orthotropic plate. They are [6]:

$$D_L = \frac{E_L t_p^3}{12\left(1 - \nu_L \nu_T\right)} \quad (4)$$

$$D_T = \frac{E_T t_p^3}{12\left(1 - \nu_L \nu_T\right)} \quad (5)$$

$$D_{LT} = \frac{\nu_T E_L t_p^3}{12\left(1 - \nu_L \nu_T\right)} \quad (6)$$

$$D_s = \frac{G_{LT} t_p^3}{12} \quad (7)$$

In eqs. (4)-(7) t_p is the thickness of the panel (it is either t_f or t_w in Figure 3).

If $\sigma_{\text{Loc,flange}}/(E_L)_f < \sigma_{\text{Loc,web}}/(E_L)_w$, the flange buckles first. The buckling stress for I-flange is approximated by [2]:

$$\sigma_{\text{Loc,a}} = \frac{1}{\left(b_f / 2\right)^2 t_f}\left(7\sqrt{\frac{D_L D_T}{1 + 4.12\zeta_{\text{I-flange}}}} + 12 D_s \right) \quad (8)$$

$$\text{Where } \zeta_{\text{I-flange}} = \frac{\left(D_T\right)_f}{k_{\text{I-flange}}\left(b_f / 2\right)} \quad (9)$$

$$\text{And } k_{\text{I-flange}} = \frac{\left(D_T\right)_w}{d_w}\left[1 - \frac{\sigma_{\text{flange}}\left(E_L\right)_w}{\sigma_{\text{web}}\left(E_L\right)_f} \right] \quad (10)$$

In eqs. (9) and (10) $k_{I\text{-}flange}$ is a spring constant for the torsional restraint along the flange-web junction and $h_w(=h\text{-}t_f)$ is the depth of the web panel. For a channel, $b_f/2$ is replaced by b_f in eqs. (8) and (9) and $k_{\text{I-flange}}$ is double that in eq. (10) as the web is retrained by only one flange outstands rather than by two flange outstands as in the I-section.

If $\sigma_{\text{Loc,flange}}/(E_L)_f > \sigma_{\text{Loc,web}}/(E_L)_w$, the web buckles prior to the flanges. The expression for buckling stress is [2], [6]:

$$\sigma_{\text{Loc,a}} = \frac{\pi^2}{h_w^2 t_w}\left[\begin{array}{l} 2\sqrt{D_L D_T\left(1 + 4.14\xi_{\text{I-web}}\right)} \\ +\left(D_{LT} + 2D_s\right)\left(2 + 0.62\xi_{\text{I-web}}^2\right) \end{array} \right] \quad (11)$$

$$\text{Where } \xi_{\text{I-web}} = \frac{1}{1 + 10\zeta_{\text{I-web}}} = \frac{1}{1 + 10\left[\left(D_T\right)_w / k_{\text{I-web}} d_w\right]} \quad (12)$$

The torsional spring restraint $k_{\text{I-web}}$ is:

$$k_{\text{I-web}} = \frac{4\left(D_T\right)_f}{b_f}\left[1 - \frac{\sigma_{\text{Loc,web}}\left(E_L\right)_f}{\sigma_{\text{Loc,flange}}\left(E_L\right)_w} \right] \quad (13)$$

The eq. (2) requires the half-wave length a, which can only be determined by FEA or by testing. The author has carried out FEA by ABAQUS® to find an approximated value of half-wave length for each section. The imperfections were not accounted for in this research and the solution was only an eigenvalue (linear) analysis. The elastic local buckling load

$P_{Loc,FEA}$ is also determined. The columns analysed have heights from 600 mm to 800 mm.

The flange and web panels of the Pultruded FRP section are modelled as a single layer of transverse isotropic material using 8-node thick shell elements S8R [7]. The input of the material properties requires three moduli of elasticity E_L, E_T,G_{LT} and the major Poisson's ratio ν_{LT} [8].

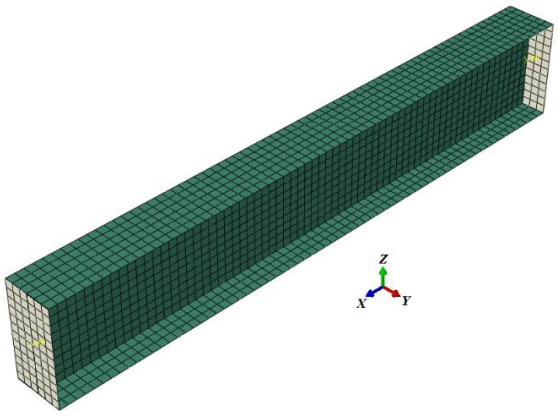

Figure 4. FE Cartesian coordinate and clamp-ended boundary condition.

To simulate a clamp-ended condition two rigid plates were fixed to both ends of the column as seen in Figure 4. The movement of each plate is controlled by a reference point located on that plate. By using Multi-Point Constraints (MPCs) to tie the reference node (acting as a 'master' point) and the edges of the section (acting as 'slave' points), the movement of all 'slave' points on the edges were numerically controlled by the 'master'. By imposing the six displacements degree of freedom at one reference node to be $U_y = U_z = U_{Rx} = U_{Ry} = U_{Rz} = 0$ and $U_x = U_y = U_z = U_{Rx} = U_{Ry} = U_{Rz} = 0$ at the other node, the required BCs were specified. The compression load was applied to the reference node having $U_x \neq 0$. Linear (bifurcation) analysis was carried to obtain the eigenvalue (critical load factor) and the buckling mode shape for local buckling failure.

For the I-section (120×60×6 mm), Figure 5 shows the local buckling mode shapes for stub columns having lengths of 600 mm,700 mm and 800 mm. It is observed that at the height of $H = 700$ mm there are four half-wave lengths. It has been recommended by Mottram[1] that to eliminate the effect of end boundary conditions on the local buckling stress the height in testing should not be shorter than four half-wave lengths.

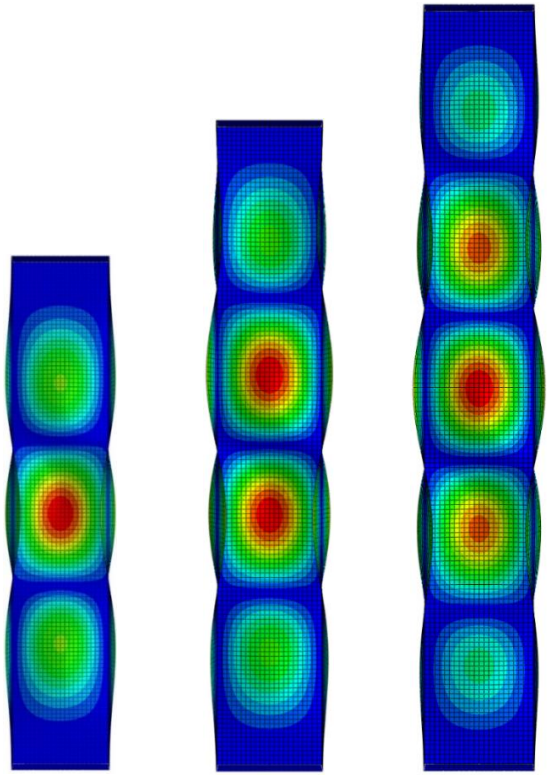

(a) (b) (c)

Figure 5. Local buckling shape of I column, heights of: (a) $H = 600$ mm; (b) $H = 700$ mm; (c) $H = 800$ mm (not to scale).

The height of the I-column was chosen to be 700 mm. FE Simulation was carried out with the C1- and C2-sections (dimension of C1 and C2 section is shown in Figure 6) to establish that H for four half-waves is $H = 750$ mm for C1 and $H = 700$ mm for C2. The local buckling load from the eigenvalue analysis $P_{Loc,FEA}$ is 251 kN, 154 kN and 172 kN for the I-, C1- and C2-sections, respectively. The approximated half-wave length a is 160 mm for the I- and C2-sections and 180 for C1.

Table 1 summarizes the required input data taken from [8] for sections I, C1, C2. The parameters include the nominal geometrical properties and the flange and web elastic constants. By adopting Eqs (2) - (13), it is found that, for I column, the web buckled prior to the

flanges and the failure stress is at 151 MPa. For C1- and C2-sections, the buckling first happens in the flanges having the failure stress of 100 MPa and 129 MPa, respectively.

Table 1. Properties to predict $\sigma_{\text{Loc,a}}$.

	I section	**C1 section**	**C2 section**
	Dimension	**Dimension**	**Dimension**
t_w	6 mm	6 mm	6 mm
t_f	6 mm	6 mm	6 mm
h_w	114 mm	114 mm	94 mm
b_f	60 mm	50 mm	50 mm
	Flange constants	**Flange constants**	**Flange constants**
E_L	29.7 GPa	29.7 GPa	34.0 GPa
E_T	10.8 GPa	11.7 GPa	11.7 GPa
v_L	0.250	0.210	0.230
v_T	0.09	0.09	0.009
	Web constants	**Web constants**	**Web constants**
E_L	26.6 GPa	33.1 GPa	31.6 GPa
E_T	10.8 GPa	11.7 GPa	11.7 GPa
v_L	0.23	0.24	0.23
v_T	0.09	0.009	0.009

Using $P_{\text{Loc,FEA}}$s obtained from FEA, the local buckling stress for I column can be calculated as:

$$\sigma_{\text{Loc,FEA}} = \frac{P_{\text{Loc,FEA}} \times E_{\text{L,web}}}{E_{\text{L,flanges}} \times A_{\text{flanges}} + E_{\text{L,web}} \times A_{\text{web}}}$$

$$= 163 \text{ MPa}$$

Those for C1 and C2 column are:

$$\sigma_{\text{Loc,FEA}} = \frac{P_{\text{Loc,FEA}} \times E_{\text{L,flange}}}{E_{\text{L,flanges}} \times A_{\text{flanges}} + E_{\text{L,web}} \times A_{\text{web}}}$$

$$= 118 \text{ MPa}$$

and 157 MPa, respectively.

It is observed that the FEA gives relatively similar local buckling stress with those by analytical prediction with difference at 8%, 18% and 22% for I, C1 and C2 respectively.

3. Experimental set-up

For the three test specimens, Figure 6 has a line drawing and a photo showing the actual cross-sections. The back-to-back channels were attached by M12 bolts at three positions along the columns' height. Two bolts were located 50 mm from the ends whilst the third one was bolted at

mid-height of the column. After connecting the two lengths together the end surfaces were squared to ensure that the compression load can be uniformly applied over the cross-section.

The thicknesses of the top and bottom flange (t_f) are assumed to be the same and were determined on taking the mean average of the four outstand measurements. The web thickness (t_w) was determined as the mean thickness measurement at three heights (but not including the end of the web, when the fillet radii increase thickness).

Table 2 summarizes the geometric properties. Rows (1-2) are used to give beam identifier and column height *H*. Rows (3-6) list, in millimetres, the section's depth (*h*), breadth (*b*), web thickness (t_w) and flange thickness (t_f). The maximum difference between the measured values and the nominal values for *h*, *b*, t_w, and t_f is 0.9%, 0.9%, 7.1% and 1.7%.

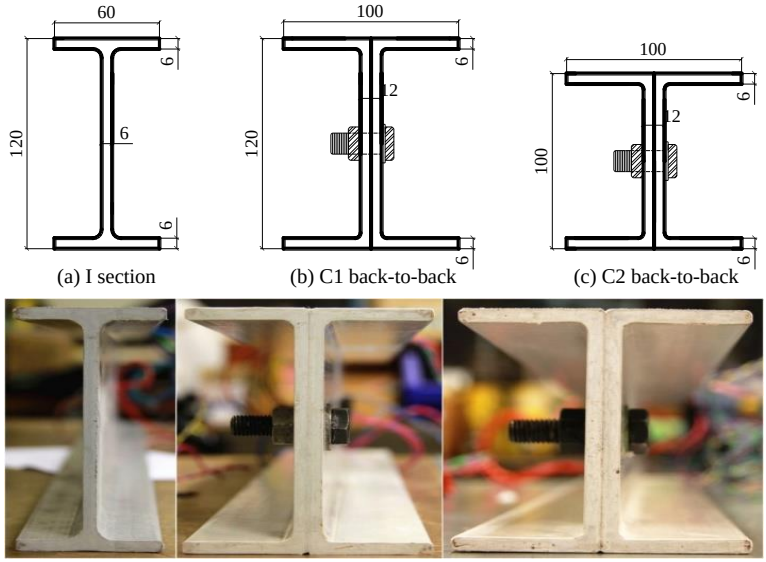

Figure 6. Drawing (top) and photo (bottom) for specimen: (a) I; (b) C1; (c) C2.

Table 2. Mean measured dimensions for I, C1 and C2.

(1)	Specimen	I	C1	C2
(2)	Height (*H*): mm	700	750	700
(3)	Depth (*h*): mm	120.1	120.1	100.1
(4)	Breadth (*b*): mm	60.05	100.9	100.8
(5)	Web thickness(t_w): mm	6.02	12.80	12.85
(6)	Flange thickness(t_f): mm	5.90	5.98	6.03
(7)	Cross-section area (*A*): mm^2	1410	2630	2360

General test arrangement is presented in Figure 7 (a) and (b). The concentric compression force was applied by a AMSLER testing machine with a full loading capacity of 40 Tonne. The machine only operates in load control. The Load was recorded by a 50 Tonne load cell placed at the bottom of the specimen. The vertical deflection was measured by having a 50 mm strain gauge displacement transducer in contact with the bottom surface the moving cross-head of the AMSLER.

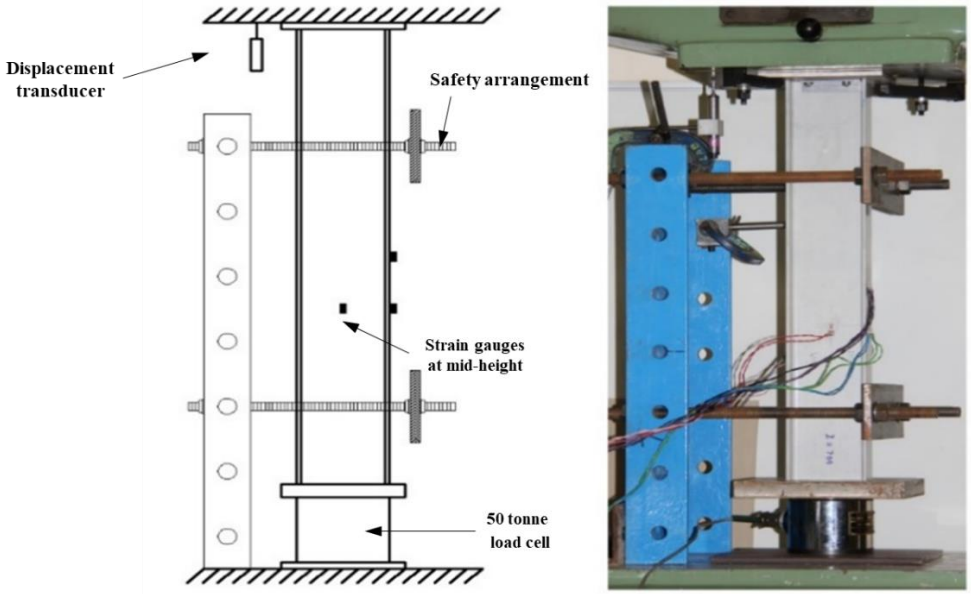

Figure 7. Colum test set-up with I-section: (a) schematics; (b) experiment.

Lateral deflection in the minor axis direction was measured by having a transducer positioned at mid-depth on the web and at the mid-height of the column. Because it was placed behind the test column, it cannot be seen in Figure 7 Six 6 mm foil strain gauges were used to measure longitudinal strain. They were attached symmetrically about the section's minor axis (the web axis). Two strain gauges were affixed to the flanges at mid-height. Four others were placed at a distance of 80 mm (for I- and C2-section) or 90 mm (for C1-section) from the mid-height on flanges and the web. The flange strain gauges (SF1 to SF4) were placed 5 mm from the flange tip, whilst the web strain gauges (SW1 and SW2) were located at mid-depth. This arrangement of gauging was based on the FEA results with the intention of capturing the maximum strain from the amplitude of the half wave-length (*a*). In Figure 7 (a) the three positions for the six strain gauges can be seen. To prevent lateral slippage at the column ends there was a steel meccano frame that, as seen in Figure 7, had four threaded bars to form a safety fixture enclosing the specimen.

4. Test results and discussion

Figure 8 (a) and (b) shows the I-section before and after there has been local buckling failure. FromFigure 8 (b), it is observed that three half wave-lengths and material rupture close to mid-height can be seen. A fourth half wave-length was visually observed near the top of the column (not shown in the photo). This deformation disappeared immediately as the load was released when FRP material fractured.

Figure 9 and Figure 10 similarly show C1 and C2 back-to-back sections during testing. It is observed that whilst the first mode was compression bearing failure, the C1 specimen failed by local buckling, the C2-section did not. At the bottom and afterwards, there was "tearing" failure along part of web-flange junction. This failure of the C2 column cannot be characterized as a local buckling instability.

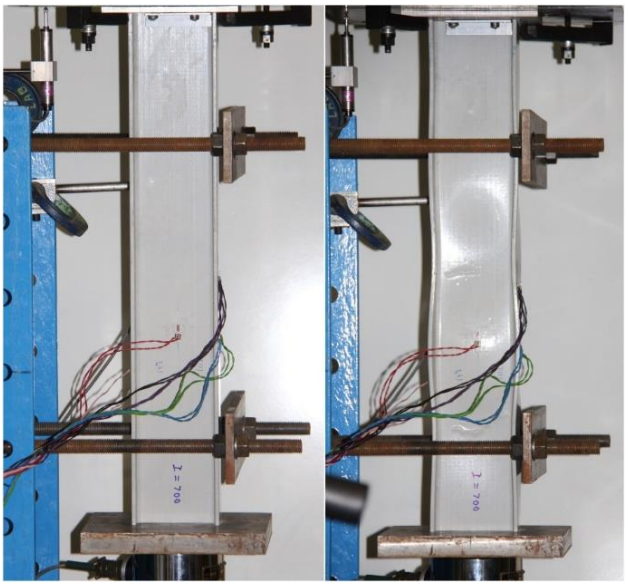

Figure 8. Local bucking test on I specimen: (a) under compression; (b) local buckling failure.

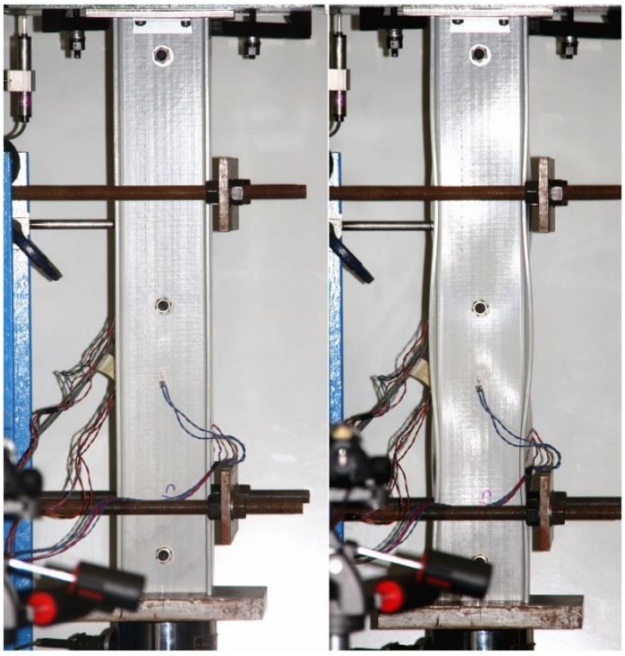

Figure 9. Local bucking test on C1 specimen: (a) under compression; (b) local buckling failure.

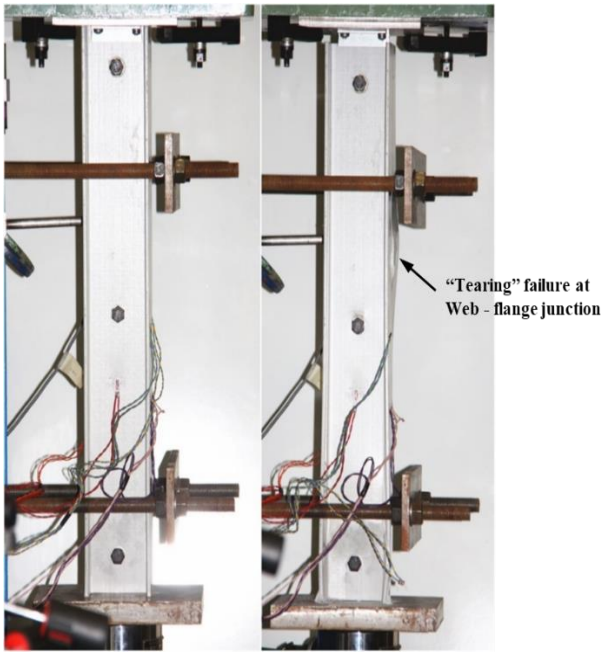

Figure 10. Local bucking test on C2 specimen: (a) under compression; (b) local buckling failure.

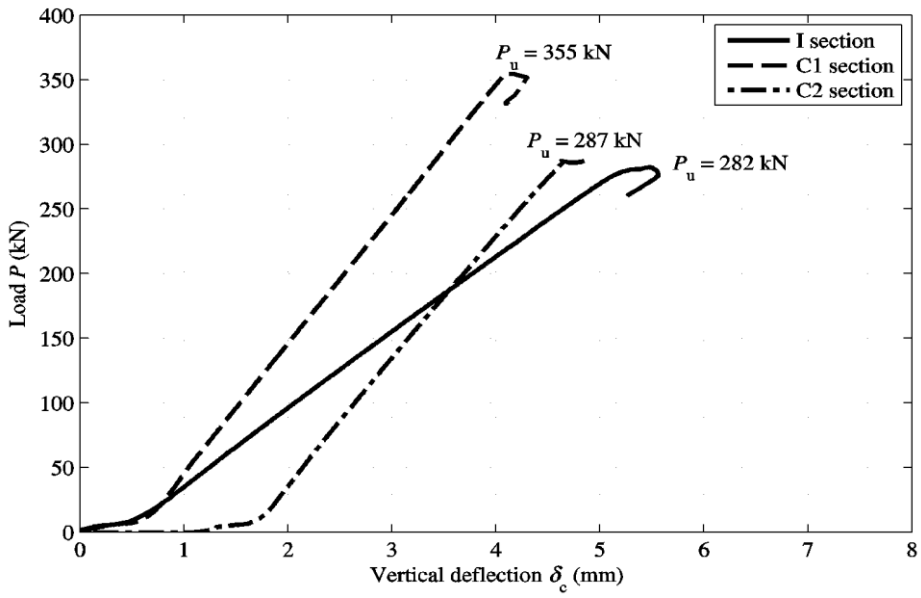

Figure 11. Load vs. vertical deflection curves for three tests

Figure 11 shows the load-vertical deflection relationships. The solid line is for the I-section, the dashed line is for the C1-section and dash-dot line is for the C2-section. The ultimate failure load (P_u) is given above the specimen's curve. P_u is for the specimen when failure had progressed into the post-buckling region. Once the specimen starts to take compression, it can be seen that P and δ_c maintains a linear relationship up to ultimate failure. It was observed at P_u that local buckling waves were visible (and obvious) with the I- and C1-sections and that there were signs of material rupture on the web or fracturing along the web-flange junctions. P_u is expected to be a higher load than when local buckling was initiated. The local buckling instability was not observed during the test with the column of section C2.

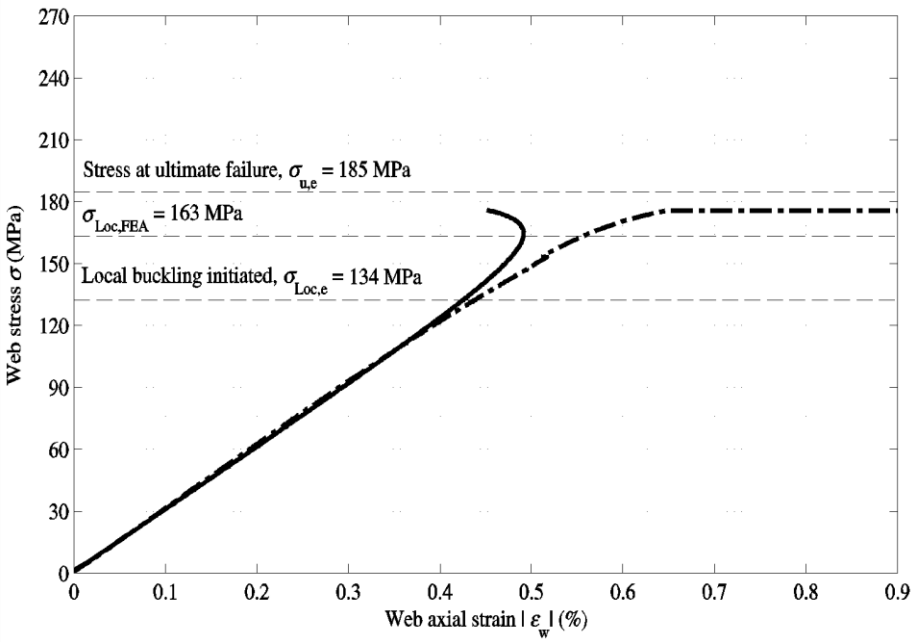

Figure 12. Web stress vs. axial strain of I column.

Figure 12 shows the two curves for web stress vs. axial strain on both sides of the web. It is observed that when $|\varepsilon_w| \geq 0.4\%$, the two strains start to diverge. The strain of one side of the web increases whilst the other decreases. This is interpreted being caused by local flexural from the onset of local (web) buckling. The three horizontal dashed-lines in the figure are for the stress at ultimate failure at $\sigma_{u,e}$ = 185 MPa the buckling stress from FEA ($\sigma_{Loc,FEA}$ = 163 MPa) and the stress at which the buckling initiated ($\sigma_{Loc,e}$ = 134 Mpa). The theoretical buckling stress obtained is $\sigma_{Loc,a}$ = 151 MPa.Theoretical prediction is 12.6% higher and the ultimate stress is 38% higher than the test results.

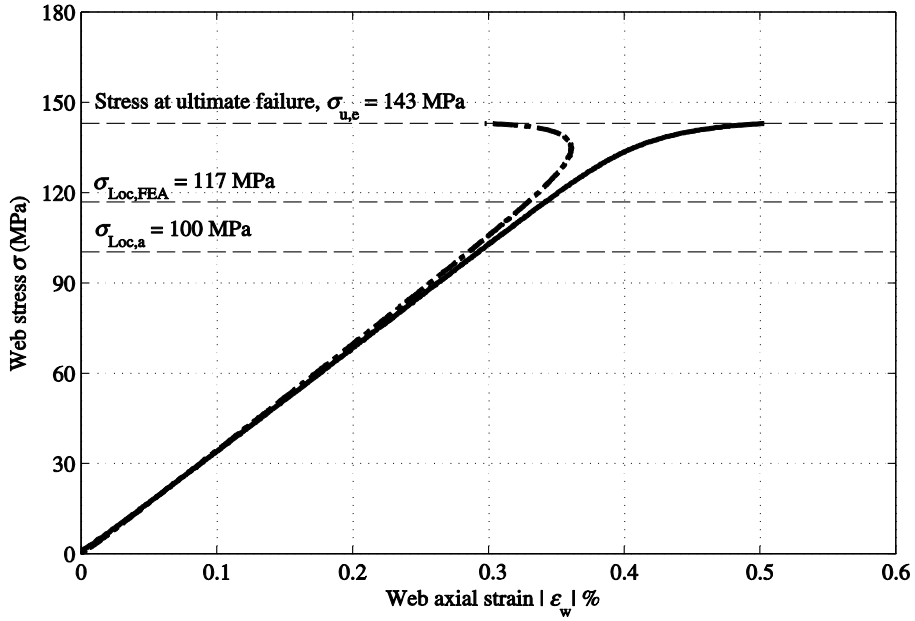

Figure 13. Web stress vs. web axial strain for C1 back-to-back specimen.

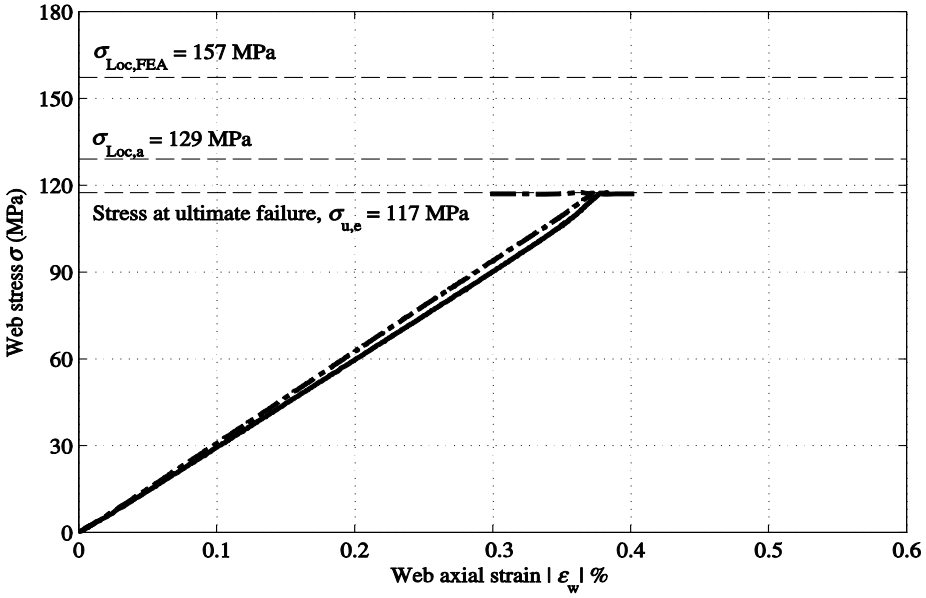

Figure 14. Web stress vs. web strain for C2 back-to-back specimen.

Figure 13 and Figure 14 give the equivalent plots using test results from the for C1 and C2 back-to-back specimen. It is observed that for C1-section, the analytical prediction gives the lowest value buckling stress with $\sigma_{Loc,a}$ = 100 MPa. At this compression stress, it is found that the strains on both sides of the web have started to diverge. This change in response indicates that a local buckling mode of failure has initiated. It is concluded that for C1 section, the theoretical prediction and the test result is similar.

It is from figure 14 for C2 section that a local buckling instability was not captured by the measurements. It is observed that when the strain exceeded 0.1% the flexure starts to contribute to the ε_w. The author believes that the local buckling stress for section C2 could be higher than that at ultimate failure $\sigma_{u,e}$ = 117 MPa. This is shown in Figure 14 is lower than those from analytical prediction ($\sigma_{Loc,FEA}$ = 157 MPa) and FEA ($\sigma_{Loc,a}$ = 129 MPa).

5. Concluding remarks

This study investigates the local buckling resistance of pultruded FRP column by comparing the predictions using Kollar's equations [2] with test results. The findings can be summarized as follows:

- Characterizing by testing of the local buckling stress for PFRP section can be difficult as this behavior is influenced by many factors such as: geometrical properties, material properties, loading distribution, column height and the rotational stiffness along the web-flange junction.
- The onset of local buckling is difficult to determine experimentally due to the fact that after the buckling occurs, there will be post-buckling resistance that allows the column to keep on resisting the increasing load without failure and the half-wave shape on the flanges or web plate does not appear to be obvious.
- The use of bolted connections to link back-to-back channels might have caused undesirable restraints that cannot be quantified in this research, which would ultimately affect the local buckling test results.
- The differences of 12.6% between theoretical predictions and test results can be acceptable. The difference between theoretical predictions and test result also comes from the fact that theoretical analysis has ignored the influence of imperfection (of material and geometry) and the rotational stiffness along the web-flange junction cannot be easily quantified in theory.

- The author finds that although the Kollar's equations can be suitable for the prediction of local buckling resistance of pultruded FRP column, it requires the half-wave length to be determined beforehand which can only be done via FEA or testing.
- The linear finite element analysis in this research has been conducted for the purpose of approximating the half-wave length of the local buckling failure. The buckling values obtained from the linear FEA in this study are for reference only. It is essential for the next research to incorporate imperfection into the FEA nonlinear analysis model.

References

[1] J. T. Mottram; "Determination of critical load for flange buckling in concentrically loaded pultruded columns". Compos. Part B: Eng. 2004; 35(1):35–47. DOI:10.1016/j.compositesb.2003.08.006.

[2] L. P. Kollár; "Local Buckling of Fiber Reinforced Plastic Composite Structural Members with Open and Closed Cross Sections". Journal of Structural Engineering. 2003; 129(11):1503–1513. DOI:10.1061/(ASCE)0733-9445(2003)129:11(1503).

[3] D. C. T. Cardoso, K. A. Harries, E. de M. Batista; "Compressive Local Buckling of Pultruded GFRP I-Sections: Development and Numerical/Experimental Evaluation of an Explicit Equation". Journal of Composites for Construction. 2015; 19(2):4014042. DOI:10.1061/(ASCE)CC.1943-5614.0000501.

[4] W. F. Ragheb; "Development of Closed-Form Equations for Estimating the Elastic Local Buckling Capacity of Pultruded FRP Structural Shapes". Journal of Composites for Construction. 2017; 21(4):4017015. DOI:10.1061/(ASCE)CC.1943-5614.0000798.

[5] T. Liu, J. D. Vieira, K. A. Harries; "Predicting Flange Local Buckling Capacity of Pultruded GFRP I-Sections Subject to Flexure". Journal of Composites for Construction. 2020; 24(4):4020025. DOI:10.1061/(ASCE)CC.1943-5614.0001032.

[6] L. C. Bank; "Composites for Construction". Hoboken, NJ, USA: John Wiley & Sons, Inc. 2006.

[7] T. T. Nguyen, T. M. Chan, J. T. Mottram, "Influence of boundary conditions and geometric imperfections on lateral–torsional buckling resistance of a pultruded FRP I-beam by FEA". Compos Struct. 2013; 100:233–242. DOI:10.1016/J.COMPSTRUCT.2012.12.023.

[8] N. . Thuy, "Lateral-torsional buckling resistance of pultruded fibre reinforced polymer shapes". Conventry, UK: University of Warwick. 2014.